Unraveling the reaction mechanism of AlCl3Lewis acid catalyzed acylation reaction of pyrene from the perspective of the molecular electron density theory

Abel Idrice Adjieufack, Anouk Gaudel-Siri, Marc Gingras, Didier Siri

NJC

ROYAL SOCIETY OF CHEMISTRY

PAPER

View Article Online
View Journal | View Issue

Cite this: *New J. Chem.*, 2023, **47**, 1925

Unraveling the reaction mechanism of $AlCl_3$ Lewis acid catalyzed acylation reaction of pyrene from the perspective of the molecular electron density theory†

Abel Idrice Adjieufack, *[a] Anouk Gaudel-Siri, [a] Marc Gingras [b] and Didier Siri *[a]

The reaction mechanism of $AlCl_3$ Lewis acid catalyzed acylation of pyrene with the methylacylium ion has been carried out at the ωB97X-D/6-311G(d,p) level within the Molecular Electron Density Theory (MEDT). Before completing this work, CDFT (Conceptual DFT) analysis allows the classification of both reactants as a nucleophile (pyrene) and super electrophile (methylacylium ion), respectively, permitting this acylation to take place with a polar character. This polar character has been supported by the high value of Global Electron Density Transfer (GEDT) recorded for each transition state. Concerning the bond changes, Bonding Evolution Theory (BET) analysis reveals that a series of four Structural Stability Domains (SSDs) are required to describe the formation of new C–C and H–Cl single bonds. For the formation of C–C single bond due to the attack of the methylacylium ion on pyrene, the first two stages correspond to (1) the creation of a pseudoradical center on both C carbon atoms (appearance of a V(C) basin) of each reactant and (2) the creation of a new C–C single bond *via* the merger of these two previous V(C) basins. Finally, the formation of a H–Cl molecule occurs *via* cleavage of an H–C bond (splitting of a V(H,C) basin) and the formation of a new H–Cl single bond (appearance of a new V(H,Cl) disynaptic basin), and the last step illustrates the restoration of the aromaticity of the ring engaged in the acylation reaction.

Received 17th October 2022,
Accepted 7th December 2022

DOI: 10.1039/d2nj05088a

rsc.li/njc

1. Introduction

Discovered in 1877[1] by Charles Friedel and James Crafts, Friedel–Crafts acylation reactions are among the major organic chemical reactions, allowing the activation of C–H bonds and formation of C–C bonds. By adding an acyl group (*via* an acylium ion) to an aromatic molecule, Friedel–Crafts acylation reactions are basic reactions to synthesize a variety of products such as aryl ketones and heterocyclic aromatic ketones.[2] From a mechanistic point of view, the first step of the Friedel–Crafts acylation consists of the generation, in the presence of a Lewis acid (LA) such as $AlCl_3$ or $FeCl_3$ (catalysts), a carbocation know as an acylium ion, which will act as electrophile in contact with aromatic compounds.[3,4] During the next step, which corresponds to aromatic ring attack by a carbocation, a tetrahedral cationic intermediate is formed, while the last step deals with the deprotonation of this intermediate in order to restore the ring aromaticity and to regenerate the LA catalyst engaged in the formation of the acylium ion.

Several experimental and computational works devoted to the acylation of benzene or non-aromatic compounds can be found in the literature.[5,6] Olah *et al.*[7] experimentally carried out the acylation reaction of benzene, alkylbenzenes, and halobenzenes with acetyl halides (fluoride, chloride and bromide) and acetic anhydride in the presence of variety of LA catalysts. For the authors, the nature of the acetylating ion (fluoride, chloride or bromide) was a key parameter affecting the ortho, meta and para isomer distribution. Motiwala *et al.*[8] performed the promoted 1,1,1,3,3,3-hexafluoro-2-propanol intramolecular Friedel–Crafts acylation reaction of aryl alkyl acid chloride. The authors claimed that the simple dissolution of an arylalkyl acid chloride in 1,1,1,3,3,3-hexafluoro-2-propanol solution was the main parameter to promote this intramolecular reaction, without conventional catalysts like the Lewis acids that are usually required for Friedel–Crafts acylation. Titinchi *et al.*[9] studied the Friedel–Crafts acetylation of 3,3′-dimethylbiphenyl coupled with the oxidation of the corresponding acetyl derivatives. Through DFT calculations of the isomeric products and the

[a] *Aix-Marseille University, CNRS, ICR, UMR 7273, CT, 13397 Marseille, France. E-mail: didier.siri@univ-amu.fr, adjieufack21@gmail.com*
[b] *Aix-Marseille University, CNRS, CINAM, UMR 7325, Marseille, France*

† Electronic supplementary information (ESI) available. See DOI: https://doi.org/10.1039/d2nj05088a

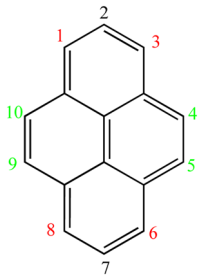

Scheme 1 Structure of pyrene containing different potential positions for EAS.

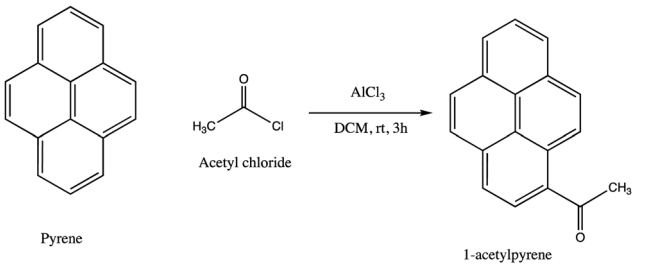

Scheme 2 Friedel–Crafts acylation between pyrene and acetyl chloride.[16]

corresponding σ-complexes, they found that the mono- and diacetylation of 3,3′-dimethylbiphenyl took place *via* different mechanisms. Melissen *et al.*[10] performed computational studies of the Al_2Cl_6-catalyzed Friedel–Crafts acylation of phenyl aromatic compounds at the ωB97X-D/6-311+G(d,p) level. They concluded that the formation of the acylium ion was the rate-determining step in the different reactions studied, followed by the formation of the Wheland intermediate. Hoque *et al.*[11] investigated the synthesis of 5,6-diaroylisoindoline-1,3-dione at the ωB97X-D/6-311++G(d,p) level from the acylation reaction between phthalimide and aroyl chloride. For a reaction mechanism taking place in two steps, they found that the energy barrier of the C–C bond formation between the benzoyl cation and phthalimide was the rate-determining step of the reaction.

Like the benzene molecule, pyrene is a polycyclic aromatic compound containing four fused benzene rings (Scheme 1). It is a colorless compound that exhibits many interesting properties. Formed during the incomplete combustion of organic compounds, it is a remarkable chromophore due to its excited-state properties and the dependence of its fluorescence upon the environment.[12] Pyrene derivatives are used to make dyes, pigments and pesticides.[13] Pyrene has different potential positions for electrophilic aromatic substitution (EAS), which can be classified by ordering of reactive sites into three nonequivalent families: [1,3,6,8], [2,7] and [4,5,9,10] (Scheme 1). Positions [1,3,6,8] and [2,7] of pyrene are known as the non-K-region, whereas positions [4,5,9,10] are called the K-region. In addition, pyrene is the most reactive at the [1,3,6,8] non-K-region during EAS reactions.[14]

From the perspective of tuning its interesting properties, the pyrene unit can be involved in many organic chemistry reactions, such as electrophilic substitutions and additions. In fact, many works in the literature have been devoted to the Friedel–Crafts acylation of pyrene.[15] The Friedel–Crafts acylation of acetyl chloride leads to the formation of 1-acetylpyrene as well as of 1,3-diacetylpyrene, 1,6-diacetylpyrene, 1,8-diacetylpyrene, 1,3,6-triacetylpyrene and 1,3,6,8-tetraiacetylpyrene, which are generated from further second, third and fourth acylations. However, the first acylation with the formation of 1-acetylpyrene and its isomers (2-and 4-acetylpyrene) can be considered as a very important step because acetylpyrenes act as intermediates for the synthesis of substituted pyrenes. For example, Guesmi *et al.*[16] synthesized 1-acetylpyrene (Scheme 2) as an intermediate in the protocol of 4-(pyren-1-yl)thiazol-2-amine synthesis. Similarly to the previous work, Pan *et al.*[17] investigated the exclusive synthesis of 1-acetylpyrene with acetic anhydride by using a co-catalyst made up of a metal chloride and a Lewis acidic ionic liquid (containing 1-butyl-3-methylimidazolium chloride).

Considering that the acylation reaction of pyrene involves a C–C bond formation and the pyrene reactive sites, the main objective of this work is to provide mechanistic highlights of the bond breaking/forming process within Bonding Evolution Theory (BET).[18] BET combining Electron Localization Function (ELF)[19] and Thom's catastrophe[20] is appropriate to monitor the electron rearrangement along reaction pathways.[21] Using BET as well as the analysis of reactivity indices defined in the framework of Conceptual DFT[22–24] and QTAIM (Quantum Theory of Atoms in Molecule),[25] Domingo proposed the Molecular Electron Density Theory (MEDT).[26] MEDT is a reactivity theory using the analysis of electron density to explain the reactivity of molecules in organic chemistry. Before achieving the above, an exploration of the potential energy surface (PES) considering the [5,6,7] reactive sites of pyrene in order to support experimental outcomes leading exclusively to acetyl pyrene (**4**, see Scheme 3)[16,17] will be carried out at the ωB97X-D/6-311G(d,p) level in the framework of MEDT. Finally, analysis of electron density variations associated with the most favorable reaction pathway is carried out in order to describe: (1) how the electron density rearrangement takes place during the process and (2) how the electron flow accompanies the bond breaking/forming processes.

2. Computational methods

Full geometry optimizations were carried out using the ωB97X-D functional[27] which includes long-range exchange and London-dispersion correction as implemented in the Gaussian 16 package[28] together with the 6-311G(d,p) basis set. The nature of each stationary point on the PES was verified by a frequency calculation at 298 K and 1 atm. Minima (reactants, intermediates, and products) were characterized by real vibration frequencies, while only one imaginary frequency was identified for transition states. In addition, Intrinsic Reaction Coordinate (IRC) calculations[29] were also performed using the Gonzalez–Schlegel algorithm[30,31] in order to verify the interconnectivity between transition states and minima.

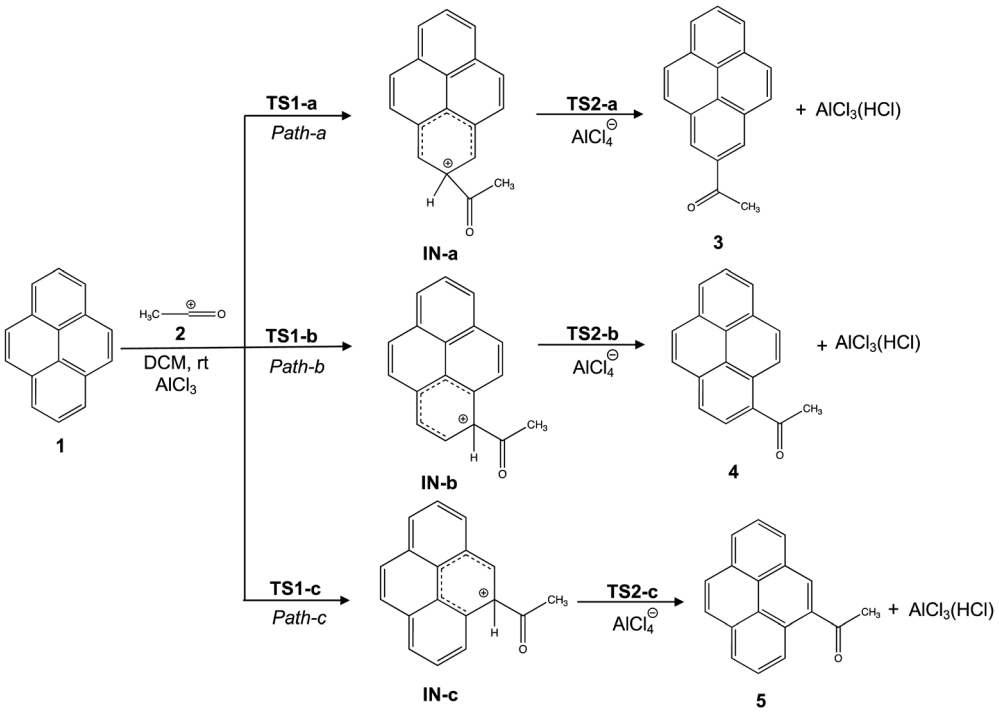

Scheme 3 Competitive reaction pathways associated with the acylation of pyrene (**1**) with the methylacylium ion (**2**).

Dichloromethane (solvent) was taken into account in all calculations using the polarizable continuum model (PCM)[32] as implemented in Gaussian 16.

Global Electron Density Transfer (GEDT)[33] for each transition state was estimated *via* the natural population analysis[34,35] using the equation $\mathrm{GEDT}(f) = \sum_{q \in f} q$, where q are the atoms of a fragment (f) belonging to the TSs. Conceptual DFT (CDFT) reactivity indices,[22,24] namely, electronic chemical potential (μ), global electrophilicity index (ω) and chemical hardness (η), were calculated through the equations given according to ref. 24, while the nucleophilicity index (N) was defined as $N = E_{\mathrm{HOMO}}(\mathrm{Nu}) - E_{\mathrm{HOMO}}(\mathrm{TCE})$, where tetracyanoethylene (TCE) was used as a reference in the context of polar organic reactions.[36]

For the topological analysis within the BET theory at the ωB97X-D/6-311G(d,p) level, the wavefunction was extracted at each point of the IRCs, and ELF analysis was performed using the TopMod package[37] considering a cubic grid of 0.2 Bohr. The ELF basin positions, as well as the ELF of selected basins, were visualized using the DrawMol and DrawProfile codes.[38]

3. Results and discussion

3.1. ELF topology analysis of pyrene 1 and methylacylium ion 2

ELF topology,[18,39] which permits the characterization of the chemical bonds of molecules, was carried out to assess the electronic structure of pyrene and the methylacylium ion. Fig. 1 displays the key ELF basin attractor positions and valence basin populations found in both reactants and engaged in the acylation reaction between pyrene (**1**) and the methylacylium ion (**2**).

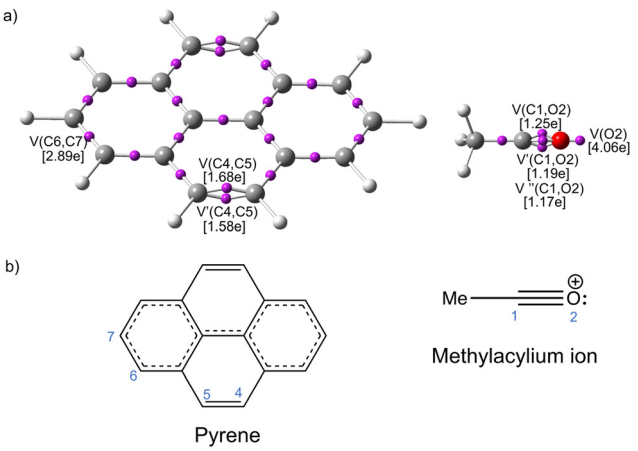

Fig. 1 (a) Representation of electron localization function (ELF) attractors and valence basin populations, in e, and (b) the proposed Lewis structures for pyrene (**1**) and the methylacylium ion (**2**).

In methylacylium ion (**2**), we note the presence of three V(C1,O2) disynaptic basins with electron populations of 1.25[V(C1,O2)], 1.19[V′(C1,O2)] and 1.17[V″(C1,O2)]e, respectively, and representing the three C–O single bonds between C1 and O2 atoms. In addition, there is one V(O2) monosynaptic basin with a population of 4.06 e, which is associated with the non-bonding electron density on the O2 oxygen (two lone pairs). On the other hand, at the k-regions **1** and **2** pyrene presents one disynaptic basin, V(C6,C7), describing the C6–C7 aromatic bond with a population of 2.89 e, while at k-regions 4 and 5, it shows two disynaptic basins, V(C4,C5) and V′(C4,C5), which have density populations of 1.68 and 1.59 e, respectively.

The presence of these two basins illustrates the distinct behaviour of the C–C double bond, which is not engaged in the aromaticity of the apical rings to which it is connected.

3.2. Analysis of the CDFT indices of pyrene 1 and methyl acylium ion 2

The CDFT indices, namely, electronic chemical potential (μ), chemical hardness (η) electrophilicity index (ω) and nucleophilicity index (N), are key tools for a better understanding of the reactivity of various of the reactants involved in the process of polar reactions like Diels–Alder and 32CA ([3+2] cycloaddition) reactions.[22,24]

The electronic chemical potential of pyrene (**1**), $\mu = -3.40$ eV, is higher than that of the methylacylium ion ($\mu = -13.76$ eV; Table 1). This observation suggests that the global electron-density transfer (GEDT)[33] will take place from pyrene to methylacylium if the chemical acylation reaction between the two reactants has a polar character.

Pyrene (**1**), with a nucleophilicity index of 3.79 eV and an electrophilicity index of 1.52 eV, can be classified as a strong nucleophile and a moderate electrophile according to the well-established nucleophilicity and electrophilicity scale of Domingo.[33] On the other hand, the methylacylium ion (**2**), with a nucleophilicity index of −9.75 eV and an electrophilicity index of 9.28 eV, is classified as a poor nucleophile and a very strong electrophile. The very high value of 9.28 eV for the electrophilicity index classifies the methyl acylium ion (**2**) as a superelectrophile.[40]

In order to determine the most nucleophilic and electrophilic centers in pyrene (**1**) and the methylacylium ion (**2**), respectively, we analyzed the Parr function[33] originating from the changes in electronic density of the nucleophile and electrophile, as shown in Fig. 2. In the pyrene molecule, the C6 atom (see Fig. 1) is the most nucleophilic atom, with a Parr nucleophilic function (P_k^-) value of 0.24 and a corresponding nucleophilic index N_k of 0.91 eV. For the methylacylium ion (**2**), the C1 carbon atom is the most electrophilic center with ω_k = 6.40 eV. The C4 and C5 atoms (P_k^- = 0.09) are much poorer nucleophiles with a nucleophilic index N_k of 0.34 eV. This value, which is about three times lower than that of C6, can justify why pyrene is much less reactive or not reactive at these positions during electrophilic substitution reactions.[14]

3.3. Energetic and geometrical analysis

The acylation reaction of pyrene with the methylacylium ion takes place through a stepwise mechanism with the formation of molecular complexes (**MC-x**) and tetrahedral cationic intermediates (**IN-x**) *via* reaction paths **a**, **b** and **c**, leading to the formation of 7-, 6-, and 5-acetylpyrene (**3**, **4** and **5**), respectively (Scheme 3).

Table 1 B3LYP/6-31G(d) electronic chemical potential, μ; chemical hardness, η; electrophilicity, ω; and nucleophilicity, N, in eV

Species	μ	η	ω	N
1	−3.40	3.85	1.52	3.79
2	−13.76	10.20	9.28	−9.75

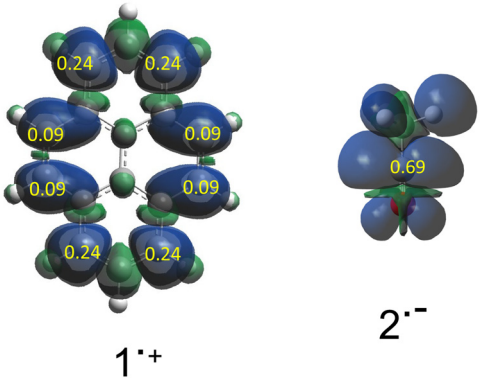

Fig. 2 Parr nucleophilic (P_k^-) and electrophilic function indices (P_k^+) of pyrene (**1**) and the methylacylium ion (**2**).

Along each reaction path, the first step corresponds to the electrophilic attack of the acylium ion on pyrene with the formation of **MC-x** and then **IN-x** *via* transition state structure **TS1**. The second step corresponds to the deprotonation of **IN-x** by the tetrachloroaluminate ($\mathbf{AlCl_4^-}$) anion *via* the transition state structure **TS2**. The relative energies and thermodynamic data of all species involved in this acylation reaction are given in Table 2.

The enthalpy values associated with the formation of the molecular complex along the three paths (**a–c**) are similar at −5.5 (**MC-a**), −5.9 (**MC-b**) and −5.5 (**MC-c**) kcal mol^{-1}, respectively. The corresponding activation enthalpy barriers to be overcome are 7.0 (**TS1-a**), 3.1 (**TS1-a**) and 3.3 (**TS1-c**) kcal mol^{-1}, see Fig. 3. In addition, the formation of **IN-x** is exothermic in all three cases, with reaction enthalpy values of −6.0 (**IN-a**), −19.5 (**IN-b**) and −11.7 (**IN-c**) kcal mol^{-1}, respectively. The most favourable reaction pathway is path-**b**, in good agreement with the CDFT index analysis, which suggested the most favourable interaction between the acylium ion and pyrene C2 carbon atom. Indeed, the transition state structure **TS1-b** is 3.9 and 0.2 kcal mol^{-1} lower than **TS1-a**(path-**a**) and **TS1-c**(path-**c**), respectively. The conversion of **IN-x** into substituted pyrene (**3–5**) with the release of the catalyst ($AlCl_3$) along each reaction pathway must overcome an activation barrier of 2.5 (**TS2-a**), 17.4 (**TS2-b**) and 11.8 (**TS2-c**) kcal mol^{-1}. Unlike in the previous step (electrophilic attack), **TS2-a** is the most favourable transition state structure; it is 14.9 and 9.3 kcal mol^{-1}

Table 2 Relative energies (in kcal mol^{-1}) of all species involved in the acylation reaction at the ωB97X-D/6-311G(d,p) level in DCM

	Path-**a**		Path-**b**		Path-**c**	
Species	ΔH°	ΔG°	ΔH°	ΔG°	ΔH°	ΔG°
MC-x	−5.5	4.8	−5.9	4.9	−5.5	6.5
TS1	1.5	13.6	−2.8	9.1	−2.2	10.0
IN-x	−11.5	7.5	−25.4	−5.3	−17.2	2.8
TS2	−9.0	13.4	−8.0	14.2	−5.4	16.5
Acyl-pyrene	−12.0	8.5	−36.4	−13.6	−35.0	−11.8

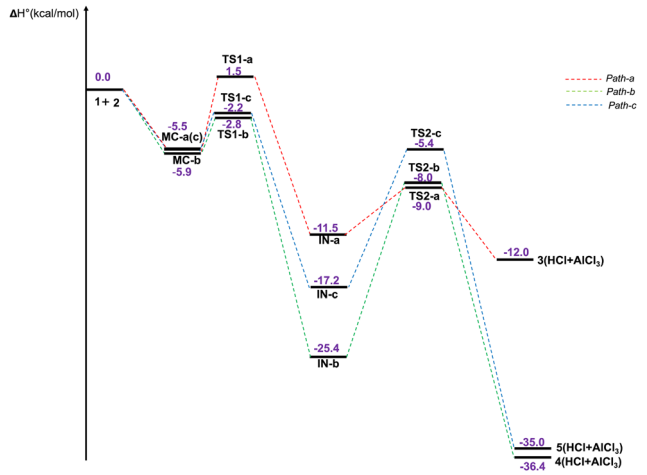

Fig. 3 Relative enthalpy energy profile along the three competitive paths (**a**, **b**, and **c**), in kcal mol^{-1}, for the stationary points involved in the Friedel–Crafts reaction of pyrene (**1**), evaluated at the ωB97X-D/6-311G(d,p) level and in DCM.

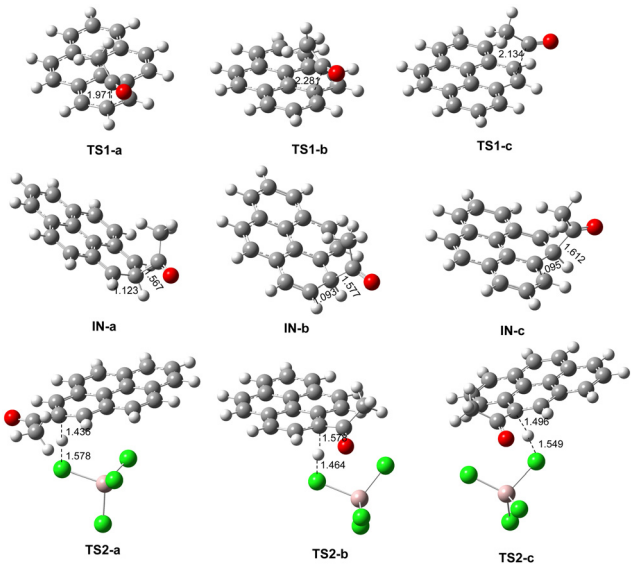

Fig. 5 ωB97X-D/6-311G(d,p) geometries of the **TSs** and **IN-x** involved in the Friedel–Crafts acylation of pyrene (**1**) by the methylacylium ion (**2**).

lower than those along reaction path-**b** and path-**c**. Finally, substituted pyrene is obtained through a globally exothermic process that corresponds to −0.5 (**3**), −11.0 (**4**) and −17.8 (**5**) kcal mol^{-1} (Table 2).

For the Gibbs free energy, the same observations are noted, with path-**b** being more favourable than path-**a** and path-**c**, see Fig. SI1 (ESI†). Fig. 4 displays the Gibbs free energy profile for path-**b** with an endergonic formation of the complex **MC-b** by 4.9 kcal mol^{-1}.

Fig. 5 displays the geometries of the transition states found in the acylation reaction calculated at the ωB97X-D/6-311G(d,p) level in dichloromethane (DCM). For the first series of transition state structures, **TS1**, corresponding to the electrophilic attack of methyl acylium ion (**2**) on pyrene (**1**), the length of the new C–C single bond is 1.971 Å at **TS1-a**, 2.281 Å at **TS1-b** and 2.134 Å **TS1-c**. Based on the previously described energetic features, a relationship can be established between the C–C distance and the activation free energy. The longest C–C bond corresponds to the earliest and least-energetic TS. The C–C and C–H distances found in the three **IN-x** are 1.567 and 1.123 Å in **IN-a**, 1.577 and 1.093 Å in **IN-b** and 1.612 and 1.095 Å in **IN-c**. Finally, for the second series of transition state structures, **TS2**, corresponding to the tetrachloroaluminate-anion-promoted deprotonation of each **IN-x**, the C–H and Cl–H bond lengths are 1.436 and 1.578 Å in **TS2-a**, 1.578 and 1.464 Å in **TS2-b** and 1.496 and 1.549 Å in **TS2-c**. By using the geometrical parameters of the TSs for the deprotonation of **IN-x**, the asynchronicity can be estimated as $\Delta l = |d(\text{C–H}) - d(\text{Cl–H})|$. The Δl values are 0.14 Å for **TS2-a**, 0.11 Å for **TS2-b** and 0.05 Å for **TS2-c**, suggesting that **TS2-a** has a stronger asynchronous character than **TS2-b** and **TS2-c**. This could be due to the steric interaction between the tetrachloroaluminate anion ($\mathbf{AlCl_4^-}$) and the methylcarbonyl group of **IN-b**, which increases the C–H distance in **TS2-b** by 0.14 and 0.08 Å (compared to those in **TS2-a** and **TS2-c**).

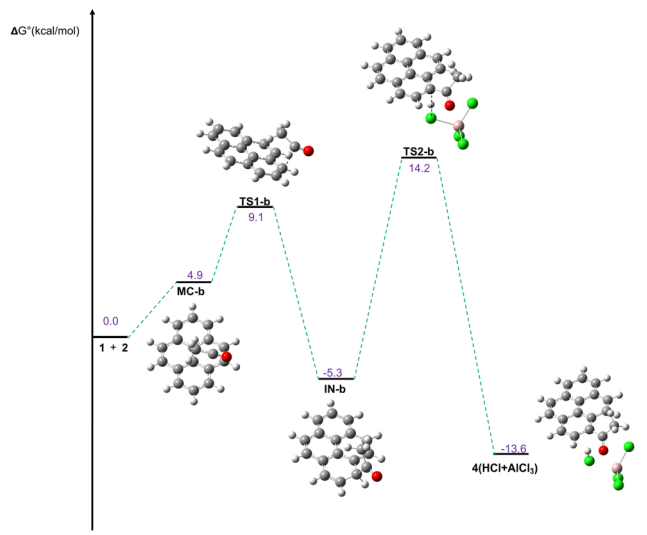

Fig. 4 Relative Gibbs free energy profile (path-**b**), in kcal mol^{-1}, for the stationary points involved in the Friedel–Crafts reaction of pyrene (**1**), evaluated at the ωB97X-D/6-311G(d,p) level and in DCM.

The computed GEDT value of the framework of the transition state structure is a powerful tool to evaluate the polar character of organic reactions. For this Friedel–Crafts reaction, the GEDT values are 0.51 e for **TS1-a**, 0.72 e for **TS1-b** and 0.59 e for **TS1-c**, while for the second series of transition state structures, they are 0.62 e for **TS2-a**, 0.53 e for **TS2-b** and 0.60 e for **TS2-c**. These computed values of GEDT reveal the polar character of this Friedel–Crafts reaction according to Domingo,[41] who defined polar reactions as those with a GEDT value higher than 0.20 e.

3.4. BET analysis during the attack of the electrophilic methylacylium ion (2) on pyrene *via* reaction path-b

Considering energetic aspects, path-**b** is the most favourable pathway for the acylation reaction between pyrene (**1**) and the

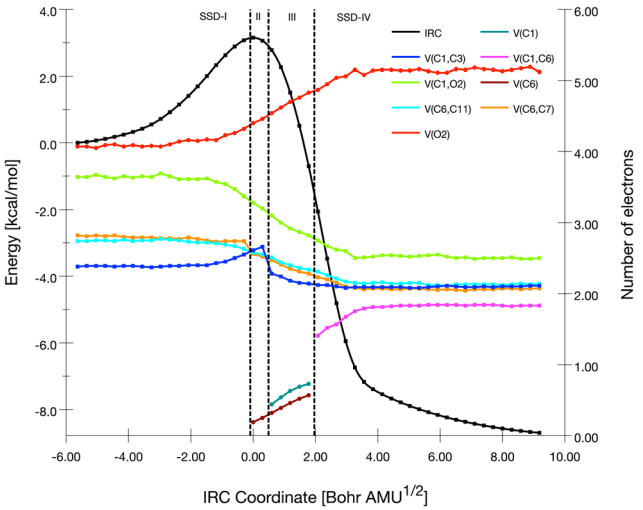

Fig. 6 Population evolution (in electrons) of selected basins along the IRC path corresponding to path-**b** (**TS1-b**).

methylacylium ion (**2**). We also carried out analysis of the bond breaking/forming process within bond evolution theory (BET). Fig. 6 displays the evolution of the density population of the different atoms engaged in the formation of the new C–C single bond. For the formation of this new C–C bond, a series of four structural stability domains (SSDs) is required (Fig. 7). The first domain, SSD-I [d(C1–C6) = 3.029 Å], contains the key atomic basins of the key atoms and their electron populations for both reactants. Pyrene presents two disynaptic basins, V(C6,C7) and V(C6,C11), with electron populations of 2.82 and 2.74 e, respectively, and corresponding to the two aromatic C6–C7 and C6–C11 bonds. In addition, in the framework of the methyl acylium ion, we note one monosynaptic V(O2) with a population of 4.07 e, and two disynaptic basins V(C1,O2) [3.64 e] and V(C1,C3) [2.38 e] found between the C1, O2, and C3 atoms (see Fig. 1 for atom labeling). At the end of this domain [d(C1–C6) = 2.341 Å], some basins, like V(C6,C7) [2.74 e] and V(C6,C11) [2.63 e], exhibited some fluctuations in their electron populations.

The reduction of the electron population of these basins [V(C6,C7), 2.56 e, and V(C6,C11), 2.58 e] continues at the beginning of second domain SSD-I [d(C1–C6) = 2.281 Å] with the creation a new monosynaptic basin V(C6), which illustrates the creation of a pseudoradical center on the C6 carbon atom of pyrene (**1**).[42] Its density population of 0.19 e originates from the depopulation of the V(C6,C7) disynaptic basin, which shows a loss of 0.18 e at the beginning of the domain (SSD-II). The population of the new V(C6) basin increases along the domain and reaches 0.25 e. Similarly to the creation of V(C6) in the previous domain, another monosynaptic basin, V(C1), with an electron population of 0.44 e appears at the beginning of the third domain [d(C1–C6) = 2.281 Å] in the framework of the methylacylium ion (**2**), which is needed as the first monosynaptic V(C6) [along the SSD-II domain] for the formation of the new C–C single bond (Fig. 6). It obtains its electron population from the reduction in the population of the V(C1,C3) basin, which has a population of 2.28 e at this point of the IRC. Indeed, the V(C1,C3) disynaptic basin exhibits a drop of 0.38 e compared to its population at the last point of domain-II. The two monosynaptic basins V(C1) and V(C6) are required for the formation of the C–C bond and at the end of the third domain [d(C1–C6) = 1.923 Å], and they have populations of 0.57 and 0.73 e, respectively.

Finally, the two monosynaptic basins [V(C1) and V(C6)] merge together to form a new disynaptic basin denoted as V(C1,C6), which represents the formation of a single bond between pyrene (**1**) and the methylacylium ion (**2**) during the last domain [d(C1–C6) = 2.281 Å][33] (Fig. 6). The electron population of 1.41 e of this new disynaptic basin comes from the merger of the two previous monosynaptic basins V(C6) and V(C1) appearing in the SSD-II and SSD-III domains, respectively (Table 3).

The IRC plot of the **TS1-b** pathway varies between −5.64 and 9.18 Bohr amu$^{1/2}$ while the main topological changes appear at 0.0, 0.60 and 2.08. Using these reaction coordinate values, the corresponding values of synchronicity and absolute synchronicity[43,44] are S_y = 0.91 and S_y^{abs} = 0.84, which indicate that the breaking/forming process has 84% synchronous character.

3.5. BET analysis during the deprotonation of the tetrahedral ionic intermediate *via* the reaction path-b

Similarly to the previous step related to the electrophilic attack of the methylacylium ion, we also carried out BET analysis along the deprotonation process (Fig. 8). The results clearly

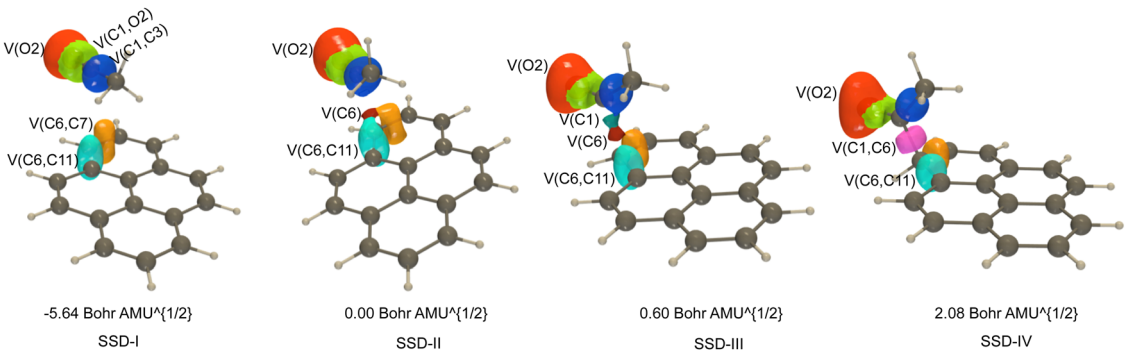

Fig. 7 ELF basin isosurfaces (η = 0.72) of each of the SSDs found along reaction path-**b** (**TS1-b**).

Table 3 Basin populations (in e), IRC coordinates (RX, amu$^{1/2}$ Bohr) and C1–C6 chemical bond lengths (in Å) along reaction path-**b** (**TS2-b**)

	SSD-I		SSD-II		SSD-III		SSD-IV	
Basins	Reactants	Last point	First point	Last point	First point	Last point	First point	Product
V(O1)	4.07	4.32	4.40	4.46	4.54	4.83	4.87	5.12
V(O1,C2)	3.64	3.37	3.28	3.20	3.10	2.82	2.75	2.50
V(C2,C3)	2.38	2.55	2.61	2.66	2.28	2.14	2.12	2.11
V(C6,C7)	2.82	2.74	2.56	2.52	2.47	2.28	2.23	2.07
V(C6,C11)	2.74	2.63	2.58	2.55	2.51	2.34	2.31	2.14
V(C1)	—	—	—	—	0.44	0.73	—	—
V(C6)	—	—	0.19	0.25	0.32	0.57	—	—
V(C1,C6)	—	—	—	—	—	—	1.41	1.83
d(C1—C6) Å	3.029	2.341	2.281	2.222	2.163	1.923	1.864	1.589
E (kcalmol^{-1})	0.00	3.07	3.15	3.06	2.78	−0.70	−2.06	−8.70
RX	−5.64	−030	0.00	0.30	0.60	1.78	2.08	9.18

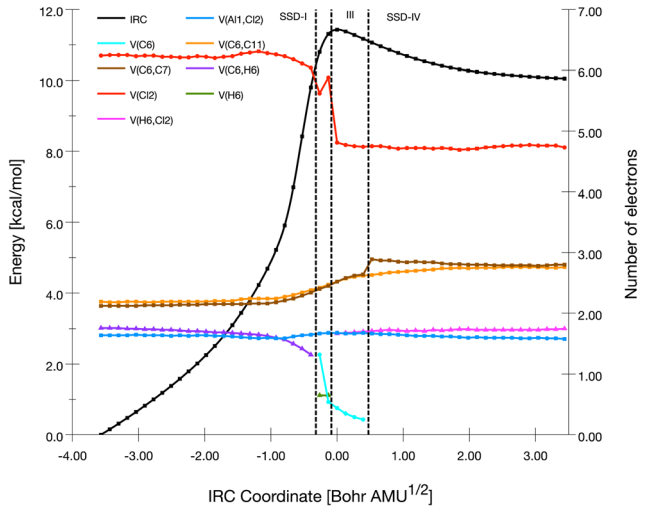

Fig. 8 Population evolution (in electrons) of selected basins along the IRC path corresponding to path-**b** (**TS2-b**).

show that the deprotonation of **IN-b** takes place within in four structural stability domains (SSDs). At the beginning of first domain [d(H6–C6) = 1.124 and d(H6–Cl2) = 2.041 Å], the main disynaptic and monosynaptic basins, namely V(C6,C7), V(C6,C11), V(H6,C6) and V(Cl2), have an electron density populations of 2.12, 2.19, 1.76 and 6.24 e, respectively. The passage from the first domain to the second one [d(H6–C6) = 1.448 and d(H6–Cl2) = 1.577 Å] is related to the disappearance of the V(H6,C6) basin in favor of the two monosynaptic basins V(H6) and V(C6). The disappearance of the V(H6,C6) basin illustrates the cleavage of the H6–C6 single bond into two *pseudoradical* centers with a positive charge on the H6 hydrogen atom and a negative one on carbon C6. The populations of the new monosynaptic basins vary from 0.65 and 1.32 e to 0.65 and 0.57 e along the domain, respectively (Table 4).

The third domain [d(H6–C6) = 1.517 and d(H6–Cl2) = 1.516 Å] starts with the disappearance of the V(H6) basin and also a high drop of 1.07 e in the population of the V(Cl2) basin. These two topological changes correspond to the formation of a new basin V(H6,Cl2), which is related to the formation of new H–Cl single bond. Its population starts at 1.67 e and ends at 1.70 e along the domain, while that of V(C6) is equal to 0.25 e. In addition, along this domain, we note the increasing populations of the V(C6,C7) and V(C6,C11) basin, which reach 2.64 and 2.62 e, respectively. The increase in the populations of these basins illustrates the transformation of the corresponding single bonds (C6–C7 and C6–C7) into double bonds. This double bond transformation ends at the beginning of the last domain SSD-IV [d(H6–C6) = 1.735 and d(H6–Cl2) = 1.378 Å] with the disappearance of the V(C6) basin (Fig. 9). They have populations of 2.80 and 2.72 e at the end of the domain (SSD-IV) due to the restoration of the aromaticity of the substituted pyrene.

The IRC curve ranges from −3.57 to 3.44 Bohr amu$^{1/2}$ along the **TS2-b** pathway with reaction coordinates of −0.26, 0.0 and

Table 4 Basin populations (in e), IRC coordinates (RX, amu$^{1/2}$ Bohr) and H6–C6/H6–Cl2 chemical bonds (in Å) along the reaction path-**b** (**TS2-b**)

	SSD-I		SSD-II		SSD-III		SSD-IV	
Basins	Reactants	Last point	First point	Last point	First point	Last point	First point	Product
V(Al1,Cl2)	1.64	1.65	1.67	1.68	1.68	1.68	1.67	1.58
V(Cl2)	6.24	6.02	5.62	5.88	4.81	4.74	4.75	4.73
V(C6,C7)	2.12	2.34	2.40	2.45	2.52	2.64	2.89	2.80
V(C6,C11)	2.19	2.38	2.42	2.47	2.52	2.62	2.63	2.76
V(H6,C6)	1.76	1.32	—	—	—	—	—	—
V(H6)	—	—	0.65	0.65	—	—	—	—
V(C6)	—	—	1.32	0.54	0.44	0.25	—	—
V(H6,Cl2)	—	—	—	—	1.67	1.70	1.71	1.75
d(H6–C6) Å	1.124	1.378	1.448	1.517	1.582	1.709	1.735	2.057
d(H6–Cl2) Å	2.041	1.642	1.577	1.516	1.464	1.387	1.378	1.328
E (kcal mol^{-1})	0.00	9.80	10.80	11.31	11.43	11.17	11.07	10.55
RX	−3.57	−0.40	−0.26	−0.13	0.00	0.40	0.53	3.44

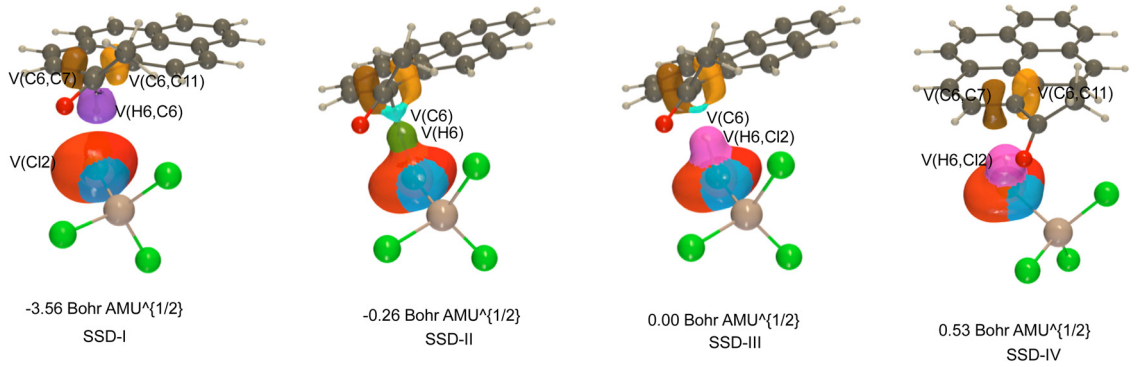

Fig. 9 ELF basin isosurfaces (η = 0.72) of each of the SSDs found along the reaction path-**b** (**TS2-b**).

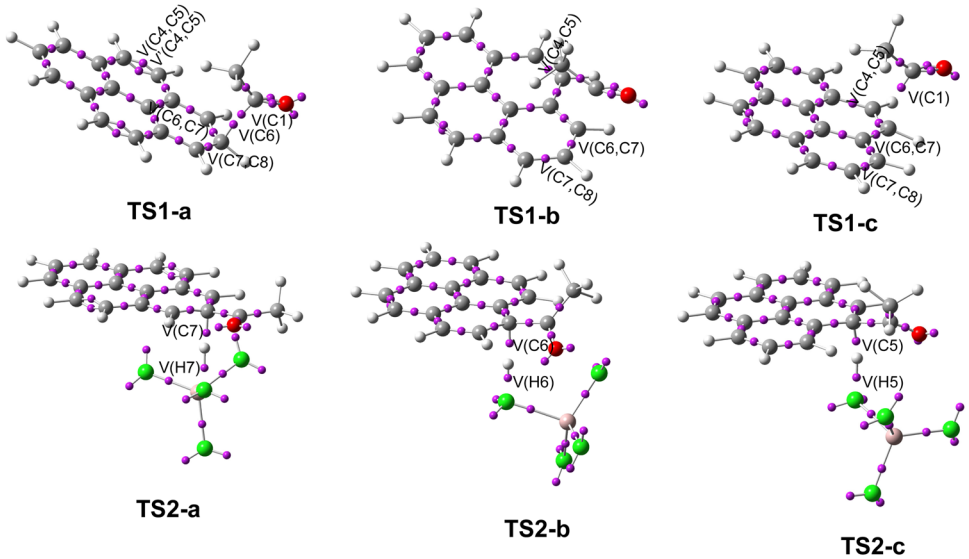

Fig. 10 ELF attractor positions of transition states **TS1-a**, **TS1-b**, **TS1-c**, **TS2-a**, **TS2-b** and **TS2-c**.

0.53 Bohr amu$^{1/2}$ related to the various bond changes, while the absolute synchronicity (S_y^{abs}) value is 0.84. Compared to the previous reaction pathway (**TS1-b**), the bond breaking/forming process taking place exhibits a slightly decreasing (84%) synchronous character.

3.6. ELF analysis of transition states involved in the acylation reaction of pyrene

Fig. 10 displays the ELF attractor basins of different transition states located along the acylation reaction between pyrene and the methylacylium ion. Relative to the ELF topology analysis of both reactants given in Section 3.1, **TS1-a** presents two new monosynaptic basins, V(C1) and V(C7), with integrations of 0.36 and 0.51 e, respectively. The two new basins are found in the framework of each reactant and illustrate the electron arrangement in the perspective of forming a new C1–C7 single bond. At **TS1-b**, there is no appearance of a new basin, but we note the merger of the two basins V(C4,C5) and V′(C4,C5) into a single one with a total of 2.89 e. The same observation is made for the transition state **TS1-c** coupled with the appearance of the new basin V(C1) [with an electron population of 0.41 e] in the framework of the methylacylium ion. Excepted certain appearance of new basin [V(C1), V(C7), and V(C1)], the presence of disynaptic basins V(Cx,Cy) related to the formation of a new C–C single bond has not been observed.

For the second series of transition states (**TS2**) related to the conversion of the tetrahedral ionic intermediate into substituted pyrenes (**3–5**), ELF analysis along the three reaction paths reveals the presence of two new monosynaptic basins, V(C) and V(H), illustrating the cleavage of the C–H single bond in the framework of the tetrahedral ionic intermediate. The two new monosynaptic basins have populations of 1.00 and 0.54 e at **TS2-a**, 0.50 and 0.67 e at **TS2-b** and 0.82 and 0.76 e at **TS2-c**. Except for these significant discrepancies, we have not noted the presence of a V(H,Cl) disynaptic basin illustrating the breakage of the C–H single bond.

4. Conclusion

The Friedel–Crafts acylation reaction of pyrene (**1**) with the methylacylium ion (**2**) has been studied within the MEDT at the

ωB97X-D/6-311G(d,p) level. In the first step, an analysis of the CDFT indices allowed pyrene (**1**) and the methylacylium ion (**2**) to be classified as a strong nucleophile and superelectrophile, respectively. In addition, the Parr functions of the two reagents account for the favourable interaction between the C1 and C6 carbon atoms of the methylacylium ion (**2**) and pyrene (**1**), respectively, leading to the final formation of 6-acetylpyrene (**4**). The activation enthalpy analysis reveals that the first step of this Friedel–Crafts acylation reaction, which corresponds to electrophilic addition, takes place with a relatively low enthalpy *via* preferred reaction path-**b** (3.1 kcal mol^{-1}).

Topological ELF analysis of the transition state associated with the electrophilic attack of the methylacylium ion (**2**) on positions **5**, **6** and **7** of pyrene (**1**) reveals that the formation of a new C–C single bond has not yet started despite the presence of some monosynaptic basins required for this formation. The presence of these monosynaptic basins can be related to the short C–C distance recorded for **TS1-a** and **TS2-c**. In addition, for the **TS2** series, which is related to the deprotonation of the tetrahedral cationic intermediates to regain the aromaticity, we observed the presence of two new monosynaptic basins, V(H) and V(C), related to the cleavage of the H–C single bond.

To understand the bond changes (breaking and forming processes) along the acylation reaction, BET was carried out. For the first step, four SSDs are required for the formation of the new C–C single bond: (1) the depopulation of the V(C6,C7) and V(C6,C11) basins in the framework of pyrene related to the appearance of the V(C) basin, (2) the appearance of another V(C) basin in the framework of the methylacylium ion and, finally, the merger of these previous V(C) into a new disynaptic basin V(C,C). Four SSDs have also been recorded for the deprotonation of the tetrahedral cationic intermediate with the creation of two new basins [V(H) and V(C)] due to H–C bond cleavage, followed by the formation of the H–Cl single bond. Finally, the last topological change corresponds to the restored ring aromaticity with the disappearance of V(C).

Conflicts of interest

The authors declare no competing financial interest.

Acknowledgements

The project leading to this publication has received funding from the Excellence Initiative of Aix-Marseille Université – A*Midex, a French ''Investissement d'Avenir'' programme. A. A. I. thanks the A*MIDEX Pyrenex, A-M-AAP-EI-17-171-170301-11.50-GINGRAS-SAT for his postdoctoral position. This work was supported by the computing facilities of the Centre Régional de Compétences en Modélisation Moléculaire (CRCMM) of Aix-Marseille Université.

References

1 C. Friedel and J. M. Crafts, *Compt. Rend.*, 1877, **84**, 1392.
2 G. A. Olah, O. Farooq, S. M. F. Farnia and J. A. Olah, *J. Am. Chem. Soc.*, 1988, **110**, 2560.
3 F. P. DeHaan, W. D. Covey, G. L. Delker, N. J. Baker, J. F. Feigon, D. Ono, K. D. Miller and E. D. Stelter, *J. Org. Chem.*, 1984, **49**, 3959.
4 P. H. Gore, *Chem. Rev.*, 1955, **55**, 229.
5 Z. Huang, L. Jin, H. Hanb and A. Lei, *Org. Biomol. Chem.*, 2013, **11**, 1810; R. H. Vekariya and J. Aubé, *Org. Lett.*, 2016, **15**, 3534; Z. Zhao, X. Tian, P. Tang, Y.-L. Ren, S. Zhao, X. Zheng and X. Cheng, *ChemistrySelect*, 2021, **6**, 1772.
6 R.-J. Tang, T. Milcent and B. Crousse, *J. Org. Chem.*, 2018, **83**, 14001; S. P. Chavan, S. Garai, A. K. Dutta and S. Pal, *Eur. J. Org. Chem.*, 2012, 6841; R. Chang, Y. Tian, N. Li, J. Bai, H. Yan, W. Yang, Z. Guo and A. Li, *Catalysts*, 2019, **9**, 141.
7 G. A. Olah, M. E. Moffatt, S. J. Kuhn and B. A. Hardie, *J. Am. Chem. Soc.*, 1964, **86**, 2198.
8 H. F. Motiwala, R. H. Vekariya and J. Aube, *Org. Lett.*, 2015, **17**, 5484.
9 S. J. J. Titinchi, F. S. Kamounah, H. S. Abbo and O. Hammerich, *Chem. Cent. J.*, 2012, **6**, 52.
10 S. T. A. G. Melissen, V. Tognetti, G. Dupas, J. Jouanneau, G. Lê and L. Joubert, *J. Mol. Model.*, 2013, **19**, 4947.
11 M. M. Hoque, M. S. Hussen, A. Kumer and M. W. Khan, *Mol. Simul.*, 2020, **16**, 1298.
12 K. Kalyanasundaram and J. K. Thomas, *J. Am. Chem. Soc.*, 1977, **99**, 2039; X. Feng, J.-Y. Hu, F. Iwanaga, N. Seto, C. Redshaw, M. R. J. Elsegood and T. Yamato, *Org. Lett.*, 2013, **15**, 1318; A. Wrona-Piotrowicz, J. Zakrzewski, R. Métivier, A. Brosseau, A. Makal and K. Wózniak, *RSC Adv.*, 2014, **4**, 56003.
13 H. I. Abdel-Shafy and M. S. M. Mansour, *Egypt. J. Pet.*, 2016, **25**, 107.
14 X. Feng, J.-Y. Hu, C. Redshaw and T. Yamato, *Chem. – Eur. J.*, 2016, **22**, 11898; Y. Niko, S. Kawauchi, S. Otsu, K. Tokumaru and G.-I. Konishi, *J. Org. Chem.*, 2013, **78**, 3196.
15 D. Zych, *Molecules*, 2019, **24**, 2551; L. Chouai, F. Wu, Y. Jang and R. P. Thummel, *Eur. J. Inorg. Chem.*, 2003, 2774; R. G. Harvey, J. Pataki and H. Lee, *Org. Prep. Proced. Int.*, 1984, **16**, 144; I.-Y. Jeon, E.-K. Choi and S.-Y. Bae, *Nanoscale Res. Lett.*, 2010, **5**, 1686; S. Hainke, S. Arndt and O. Seitz, *Org. Biomol. Chem.*, 2005, **3**, 4233; S. R. D. George, T. D. H. Frith, D. S. Thomas and J. B. Harper, *Org. Biomol. Chem.*, 2015, **13**, 9035; X. Q. Lu, M. Xing, A. X. Pan, Y. Y. Wu, J. M. Xie and M. Chen, *Adv. Mater. Res.*, 2012, **560**, 294; R. Flamholc, D. Plazuk, J. Zakrzewski, R. Métivier, K. Nakatani, A. Makal and K. Wózniak, *RSC Adv.*, 2014, **4**, 31594; A. Wrona-Piotrowicz, J. Zakrzewski, A. Gajda, T. Gajda, A. Makal, A. Brosseau and R. Métivier, *Beilstein J. Org. Chem.*, 2015, **11**, 2451.
16 N. E. Guesmi, E. M. Hussein, B. H. Asghar, R. J. Obaid, R. S. Jassas, A. Alharbi, H. M. Altass, I. I. Althagafi, M. Morad, Z. Moussa and S. A. Ahmed, *Arabian J. Chem.*, 2020, **13**, 3702.
17 A. Pan, T. He, L. Xu, Y. Fang, H. Li, J. Xie and M. Chen, *Int. J. Chem. React. Eng.*, 2013, **11**, 1.
18 X. Krokidis, S. Noury and B. Silvi, *J. Phys. Chem. A*, 1997, **101**, 7277.

19 A. D. Becke and K. E. Edgecombe, *J. Chem. Phys.*, 1990, **92**, 5397.
20 R. Thom, in *Structural Stability and Morphogenesis – an outline of a general theory of models, 1st English*, ed. W. A. Benjamin, 1975.
21 E. Cherni, A. I. Adjieufack, B. Champagne, M. Abderrabba, S. Ayadi and V. Liégeois, *J. Phys. Chem. A*, 2020, **124**, 4068; J. Andrés, S. Berski and B. Silvi, *Chem. Commun.*, 2016, **52**, 8183; J. Andrés, P. Gonzalez-Navarrete, V. S. Safont and B. Silvi, *Phys. Chem. Chem. Phys.*, 2017, **19**, 29031; P. Merino, T. Tejero, I. Delso and R. Matute, *Org. Biomol. Chem.*, 2017, **15**, 3364; J. Andrés, V. S. Safont, M. Oliva, K. L. Caster and F. Goulay, *Int. J. Quantum Chem.*, 2022, **122**, 26892; M. B. Mbah, A. I. Adjieufack, C. N. Nguimkeu, A. Malloum, A. Abouem, A. Zintchem, G. Bebga and I. M. Ndassa, *J. Mol. Graphics*, 2022, **96**, 107523; A. I. Adjieufack, J. F. Moto Ongagna, J. F. Kenmogne Tchidjoa and I. Mbouombouo Ndassa, *New J. Chem.*, 2021, **45**, 20342; A. I. Adjieufack, J. Andrés, M. Oliva and V. S. Safont, *PhysChem*, 2022, **2**, 207; A. I. Adjieufack, M. Mbah Bake, C. Nguemo Nguimkeu, J. Pilmé and I. Ndassa Mbouombouo, *ChemPhysChem*, 2021, **22**, 1792; A. I. Adjieufack, V. Liégeois, I. Mbouombouo Ndassa and B. Champagne, *RSC Adv.*, 2021, **11**, 10083; M. Mbah Bake, A. I. Adjieufack, P. Manwal, A. Mekoung, A. Abouem, A. Zintchem, G. Bebga, L. Rhyman, I. Mbouombouo Ndassa and R. Ponnadurai, *J. Comput. Chem.*, 2022, **43**, 972.
22 R. G. Parr and W. Yang, *Density Functional Theory of Atoms and Molecules*, Oxford University Press, New York, 1989.
23 P. Geerlings, F. De Proft and W. Langenaeker, *Chem. Rev.*, 2003, **103**, 1793.
24 L. R. Domingo, M. Ríos-Gutiérrez and P. Pérez, *Molecules*, 2016, **21**, 748.
25 R. F. W. Bader, *In Atoms in Molecules: A Quantum Theory*, Clarendon Press, Oxford, New York, 1990.
26 L. R. Domingo, *Molecules*, 2016, **21**, 1319.
27 J.-D. Chai and M. Head-Gordon, *Phys. Chem. Chem. Phys.*, 2008, **10**, 6615.
28 M. J. Frisch, G. W. Trucks, H. B. Schlegel, G. E. Scuseria, M. A. Robb, J. R. Cheeseman, G. Scalmani, V. Barone, G. A. Petersson, H. Nakatsuji, X. Li, M. Caricato, A. V. Marenich, J. Bloino, B. G. Janesko, R. Gomperts, B. Mennucci, H. P. Hratchian, J. V. Ortiz, A. F. Izmaylov, J. L. Sonnenberg, D. Williams-Young, F. Ding, F. Lipparini, F. Egidi, J. Goings, B. Peng, A. Petrone, T. Henderson, D. Ranasinghe, V. G. Zakrzewski, J. Gao, N. Rega, G. Zheng, W. Liang, M. Hada, M. Ehara, K. Toyota, R. Fukuda, J. Hasegawa, M. Ishida, T. Nakajima, Y. Honda, O. Kitao, H. Nakai, T. Vreven, K. Throssell, J. A. Montgomery, Jr., J. E. Peralta, F. Ogliaro, M. J. Bearpark, J. J. Heyd, E. N. Brothers, K. N. Kudin, V. N. Staroverov, T. A. Keith, R. Kobayashi, J. Normand, K. Raghavachari, A. P. Rendell, J. C. Burant, S. S. Iyengar, J. Tomasi, M. Cossi, J. M. Millam, M. Klene, C. Adamo, R. Cammi, J. W. Ochterski, R. L. Martin, K. Morokuma, O. Farkas, J. B. Foresman and D. J. Fox, *Gaussian 16, Revision A.03*, Gaussian, Inc., Wallingford CT, 2016.
29 K. Fukui, *J. Phys. Chem.*, 1970, **74**, 4161.
30 C. Gonzalez and H. B. Schlegel, *J. Phys. Chem.*, 1990, **94**, 5523.
31 C. Gonzalez and H. B. Schlegel, *J. Chem. Phys.*, 1991, **95**, 5853.
32 J. Tomasi, B. Mennucci and R. Cammi, *Chem. Rev.*, 2005, **105**, 2999.
33 L. R. Domingo, *RSC Adv.*, 2014, **4**, 32415.
34 A. E. Reed, R. B. Weinstock and F. Weinhold, *J. Chem. Phys.*, 1985, **83**, 735.
35 A. E. Reed, L. A. Curtiss and F. Weinhold, *Chem. Rev.*, 1988, **88**, 899.
36 L. R. Domingo, E. Chamorro and P. Perez, *J. Org. Chem.*, 2008, **73**, 4615; L. R. Domingo and P. Pérez, *Org. Biomol. Chem.*, 2011, **9**, 7168.
37 S. Noury, X. Krokidis, F. Fuster and B. Silvi, *Comput. Chem.*, 1999, **23**, 597.
38 V. Liégeois, DrawMol. UNamur, **www.unamur.be/drawmol**; V. Liégeois, V. DrawProfile. UNamur, **www.unamur.be/drawprofile**.
39 B. Silvi and A. Savin, *Nature*, 1994, **371**, 683.
40 P. Arroyo, M. T. Picher, L. R. Domingo and F. Terrier, *Tetrahedron*, 2005, **61**, 7359.
41 R. G. Parr, L. von Szentpaly and S. Liu, *J. Am. Chem. Soc.*, 1999, **121**, 1922.
42 L. R. Domingo and J. A. Saez, *J. Org. Chem.*, 2011, **76**, 373.
43 A. I. Adjieufack, I. Mbouombouo Ndassa, I. Patouossa, J. Ketcha Mbadcam, V. S. Safont, M. Oliva and J. Andrés, *Phys. Chem. Chem. Phys.*, 2017, **19**, 18288.
44 A. I. Adjieufack, B. Maraf Mbah, J. Ketcha Mbadcam, I. Mbouombouo Ndassa, J. Andrés, M. Oliva and V. S. Safont, *Int. J. Quantum Chem.*, 2019, **119**, 25985.

